Eur Biophys J (2012) 41:405–413
DOI 10.1007/s00249-012-0789-5

ORIGINAL PAPER

EBSA
Biophysics in Europe

Magnetic configuration model for the multicellular magnetotactic prokaryote *Candidatus* Magnetoglobus multicellularis

Daniel Acosta-Avalos · Luciana Maria dos Santos Azevedo · Taciana Salama Andrade · Henrique Lins de Barros

Received: 6 September 2011 / Revised: 26 December 2011 / Accepted: 16 January 2012 / Published online: 15 February 2012

Abstract *Candidatus* Magnetoglobus multicellularis (CMm) is a multicellular organism in which each constituent cell is a magnetotactic bacterium. It has been observed that disaggregation of this organism provokes the death of the individual cells. The observed flagellar movement of the CMm indicates that the constituent cells move in a coordinated way, indicating a strong correlation between them and showing that this aggregate could be considered as an individual. As every constituent cell is a magnetotactic bacterium, every cell contributes with a magnetic moment vector to the resultant magnetic moment of the CMm organism that can be calculated through the vectorial sum of all the constituent magnetic moments. Scanning electron microscopy images of CMm organisms have shown that the constituent cells are distributed on a helix convoluted on a spherical surface. To analyze the magnetic properties of the distribution of magnetic moments on this curve, we calculated the magnetic energy numerically as well as the vectorial sum of the magnetic moment distribution as a function of the number of cells, the sphere radius and the number of spiral loops. This distribution proposes a magnetic organization not seen in any other living organism and shows that minimum energy configurations of magnetic moments are in spherical meridian chains, perpendicular to the helix turns. We observed that CMm has a high theoretical degree of magnetic optimization, showing that its geometrical structure is important to the magnetic response. Our results indicate that the helical structure must have magnetic significance.

Keywords *Candidatus* Magnetoglobus multicellularis · Magnetotactic multicellular prokaryote · Magnetotaxis · Magnetic energy · Degree of magnetic optimization

D. Acosta-Avalos (✉) · L. M. dos Santos Azevedo · T. Salama Andrade · H. Lins de Barros
Centro Brasileiro de Pesquisas Físicas,
Rua Xavier Sigaud 150, Urca, Rio de Janeiro,
RJ CEP 22290-180, Brazil
e-mail: dacosta@cbpf.br; dacosta00@gmail.com

Introduction

Magnetotactic bacteria are flagellated microorganisms able to orient to magnetic fields. This is possible because of the presence of intracellular arrangements of magnetosomes, which are magnetic nanoparticles enveloped by a membrane (Frankel 2003; Bazylinski and Frankel 2004). The magnetic nanoparticles have been identified as the iron oxide magnetite (Fe_3O_4) or the iron sulfide greigite (Fe_3S_4) (Farina et al. 1990; Mann et al. 1990), depending on the bacterial metabolism. Each magnetotactic bacterium can be thought of as a live compass, because the magnetosome chain functions as a magnetic needle, transmitting magnetic torques to the cellular body that orientate its direction to that of the external geomagnetic field.

Candidatus Magnetoglobus multicellularis (CMm) (GeneBank EF014726) is a multicellular magnetotactic prokaryote (MMP) (Abreu et al. 2007). MMPs have been found all over the world: North America (Rodgers et al. 1990), South America (Abreu et al. 2007), Europe (Wenter et al. 2009), Asia (Zhou et al. 2011) and Australia (Fleming and James 2011). The CMm organism is spherical and composed of approximately 10–40 gram-negative cells. These cells are flagellated magnetotactic bacteria (Keim et al. 2006; Lins and Farina 1999). Each bacterium has magnetosomes composed mainly of the magnetic iron sulfide greigite (Fe_3S_4), but in some cases

magnetosomes of greigite or magnetite were observed in the same CMm (Lins et al. 2007). Each CMm contains about 300–1,000 magnetosomes, arranged in planar groups in the cytoplasm near the periphery of the microorganism and parallel to the external surface (Keim et al. 2006). Several observations by scanning electron microscopy suggest that the bacteria that compose this organism are organized following a roughly helical distribution (Keim et al. 2006; Lins and Farina 1999; Farina et al. 1983). The cells are arranged radially around an acellular internal compartment at the center of the organism. Each cell has a pyramidal shape with the base forming the outer surface of the organism. Confocal laser scanning microscopy shows that the radial cell arrangement is highly organized. The architecture observed has a biological advantage: all component cells are in contact with the outside environment and maintain contact with all the others through the internal acellular compartment (Keim et al. 2006). The CMm has a magnetic moment which aligns with the geomagnetic field in the same way as magnetotactic bacteria. This magnetic moment is the vectorial resultant of the distribution of magnetic moments of each constituent cell (Rodgers et al. 1990; Winklhofer et al. 2007). CMm organisms are very motile and reach velocities of about 70 μm/s. When a CMm organism is in the presence of a magnetic field, it is observed to swim in an elongated helical trajectory with the symmetry axis aligned to the applied magnetic field (Perantoni et al. 2009). Observations made with the magnetic field parallel to the optical axis of an optical microscope (i.e., field direction perpendicular to the microscope slide) show that during its migratory movement, the cell body rotates once in the same sense of the helical trajectory (clockwise) (Keim et al. 2006). This is evidence that the flagella of each component cell are parallel to the organism surface and create forces that produce a precession of the cellular body around the symmetry axis of the organism. It is known that CMm loses its magnetization upon exposure to demagnetizing magnetic fields, recovering it later (Rodgers et al. 1990; Keim et al. 2006), and that exposing these organisms to strong magnetic fields (about 1,000 G) remagnetizes them to higher magnetization values to about 20% of their natural ones (Winklhofer et al. 2007). These observations indicate some kind of organization of the magnetic moments associated to each magnetotactic bacterium composing CMm. In this paper we propose that the magnetic moments are arranged in a spherical helix and that the observed magnetic properties of CMm depend on this distribution. The magnetostatic energy that results from the distribution of magnetic moment vectors attached to a spiral curve is analyzed, and the magnetic moment distributions with extreme energies (minimal and maximum) are found. The biological implications of these magnetic configurations are discussed.

Mathematical model

The curve

CMm has a unique organization of cells among the prokaryotes (Keim et al. 2004a). The study of CMm organisms has produced the following observations about the cells that compound them:

1. Cells are genetically identical (Abreu et al. 2007), having a size distribution. This distribution is not too wide, being (3.1 ± 0.44) μm, as described by Lins and Farina (1999). So, it can be said that the constituent cells have similar volumes.
2. Magnetosomes are distributed in planar groups near the periphery of each CMm cell (Abreu et al. 2007).
3. The cells are joined forming a sphere but following a curve around the sphere (Abreu et al. 2007; Lins and Farina 1999; Farina et al. 1983; Perantoni et al. 2009; Silva et al. 2003) and not randomly as in the aggregation of soap bubbles (Silva et al. 2003).
4. CMm constituent cells are pyramidal in form, with the base facing the external ambient and the apex directed to the sphere center (Keim et al. 2006).
5. The coordinated movement shown for CMm organisms must be the result of a highly specialized structure that permits the cells to respond as a unit. Also, the CMm magnetization shows a degree of optimization incompatible with a random cell organization (Rodgers et al. 1990; Winklhofer et al. 2007; Perantoni et al. 2009).

Considering the preceding observations, it is feasible to propose a model for the cell organization and consequently for its magnetic organization.

Figure 1 shows a SEM micrograph of several CMm organisms with their typical architecture. In the paper by Abreu et al. (2007) the curve followed by the cells around the spherical organism is identified as spiral. Farina et al. (1983) describe the organism structure as a helicoidal arrangement. But mathematically the observed curve is a spherical spiral or a helix convoluted on a sphere. Only one parameter is necessary to describe the curve. A helix can be described by its Cartesian coordinates

$$\begin{aligned} x &= r\cos(t) \\ y &= r\sin(t) \\ z &= At \end{aligned} \tag{1}$$

where r and A are constants, and t is a parameter. To convolute this curve over a sphere of radius R, the following equations can be used:

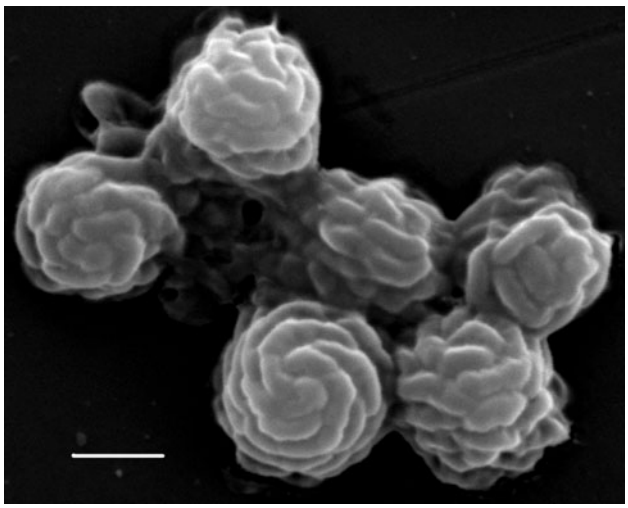

Fig. 1 Scanning electron microscopy micrograph of several *Candidatus* Magnetoglobus multicellularis organisms collected at the Araruama Lagoon, Rio de Janeiro, Brazil. The electron microscope was the Jeol JSM-5800 located at the Instituto Militar de Engenharia (IME—RJ). *Bar* = 2 μm

$$\begin{aligned} x &= \left(R^2 - z^2\right)^{1/2} \cdot \cos(t) \\ y &= \left(R^2 - z^2\right)^{1/2} \cdot \sin(t) \\ z &= [t/(L\pi) - 1] \cdot R \end{aligned} \tag{2}$$

where $-R \leq z \leq R$, $0 \leq t \leq 2L\pi$ and L is the number of loops in the helix. This parametrization is different than the common one given in spherical coordinates for a spherical helix and spherical spiral (Weisstein 2011a, b), because it maintains the cylindrical structure of Eq. 1. In this parametrization the symmetry axis of the spiral is the z axis. The spherical helix parametrization (Eq. 2) is interesting because the distance between loops is almost constant, different from the spherical spiral parametrization that produces a dense concentration of loops at the poles. Biologically, one expects an almost uniform spacing between loops, because the CMm cells have similar volumes as mentioned above. On the proposed spherical helix N cells must be distributed forming the CMm organism.

The parameters R and N are not independent. Each cell composing the organism has an average volume V_i. In the center of the organism there is an acellular internal compartment surrounded by the N cells. The total volume of the organism can be written in the following way:

$$V_T = (4/3)\pi R^3 = NV_i + V_C \tag{3}$$

Observing the TEM micrographs (for example, Fig. 6 at Keim et al. 2006) it can be assumed that $V_C \approx 0.5V_i$. The expression for R as a function of N must be:

$$R = [(3/4\pi) \cdot (N + 0.5) \cdot V_i]^{1/3} \tag{4}$$

It is assumed that V_i is approximately constant and with a value of about 0.33 μm^3 (Lins and Farina 1999).

The distribution

As magnetosomes are attached near the cell surface, it is assumed that the magnetic moment vector ($\mathbf{m}_i$) associated to each cell must be tangential to the spherical surface. As the volume occupied by the magnesome chains in the whole bacterial body is too small [$V_{magnetosomes}/V_{cell} \approx 10^{-5}$ (Lins de Barros and Esquivel 1987)], the unpaired magnetic moment can be considered as that of a point dipole. It is also common in theoretical analyses to consider magnetotactic bacteria as self-propelled magnetic dipoles (Frankel 2003). If N cells compose the organism, then N magnetic dipolar moment vectors must be distributed on the helix. As the cells are considered identical, the distance measured along the helix among adjacent magnetic dipoles, i.e., the next dipole in the helix, must be a constant. It is supposed that each magnetic moment has an inclination angle with respect to the helix curve (when the inclination angle is 0° the magnetic moment is tangent to the curve). Based on the fact that the CMm constituent cells are identical, as mentioned above, it is assumed that all the magnetic moment vectors have equal inclination angles and the same magnitude.

The energy calculation

As our interest is the magnetic energy E of the distribution in the presence of an external magnetic field B_{EXT}, it can be calculated as:

$$E = \sum_{j>i} u_{ij} - \sum_i \mathbf{m}_i \cdot B_{EXT} \tag{5}$$

where u_{ij} is the interaction energy of magnetic moments $\mathbf{m}_i$ and $\mathbf{m}_j$. The second part of Eq. 5 is related to the magnetic energy of the distribution in the presence of some external magnetic field. As all the cells are similar, it can be supposed that all the magnetic moment vectors have the same magnitude, differing only in their direction. So, it can be written:

$$\mathbf{m}_i = m_0 \mathbf{m}_{ui} \tag{6}$$

where $\mathbf{m}_{ui}$ is the unitary vector of $\mathbf{m}_i$ and represents its direction. In this way, u_{ij} can be written as:

$$u_{ij} = \left(\mu_0 m_0^2 / 4\pi r_{ij}^3\right)\left(\mathbf{m}_{ui} \cdot \mathbf{m}_{uj} - 3\left(\mathbf{m}_{ui} \cdot \mathbf{r}_{uij}\right)\left(\mathbf{m}_{uj} \cdot \mathbf{r}_{uij}\right)\right) \tag{7}$$

where $\mathbf{r}_{ij} = \mathbf{r}_j - \mathbf{r}_i$ is the relative position vector between the magnetic moments $\mathbf{m}_i$ and $\mathbf{m}_j$, $\mathbf{r}_{uij}$ is the unitary vector

of $\mathbf{r}_{ij}$, and μ_0 is the vacuum permeability. From Eq. 7 it can be seen that u_{ij} depends strongly on the relative orientation among the interacting magnetic moments. Changing the relative orientation, the energy can be changed from attractive to repulsive or vice versa.

As the magnetic moment vectors are tangent to the sphere and also have an angle with respect to the helical curve, they must be in a plane tangent to the sphere. This plane can be described by a triad of unitary vectors: the tangent vector $\mathbf{t}_i$, the normal vector $\mathbf{n}_i$ and the binormal vector $\mathbf{t}_{Pi}$. The tangent vector is calculated from its definition from the differential calculus:

$$\mathbf{t}_i = (d\mathbf{r}_i/dt) / (|d\mathbf{r}_i/dt|) \quad (8)$$

where $\mathbf{r}_i$ is calculated with Eq. 2.

The tangent plane is described by the set of perpendicular vectors $\mathbf{t}_i$ and $\mathbf{t}_{Pi}$, where

$$\mathbf{t}_{Pi} = \mathbf{t}_i \times \mathbf{n}_i \quad (9)$$

The normal vector $\mathbf{n}_i$ to the sphere is defined as $\mathbf{n}_i = \mathbf{r}_i/|\mathbf{r}_i|$, considering the sphere center as the origin of the reference system. As mentioned above, the magnetic moments do not exactly lie on the tangent direction and might be rotated for some angle α relative to the curve tangent direction (Fig. 2). As mentioned before, we suppose that all the magnetic moments have the same angle α. So, for each angle α the magnetic moment direction can be written as:

$$\mathbf{m}_{ui}(\alpha) = \cos(\alpha)\mathbf{t}_i + \sin(\alpha)\mathbf{t}_{Pi} \quad (10)$$

Equation 10 implies that the magnetic energy E is a function of α. For the N cells composing the organism, we have N magnetic moments $\mathbf{m}_i(\alpha)$ and N position vectors $\mathbf{r}_i$, and with them it is possible to calculate the magnetic energy $E(\alpha)$ using Eqs. 5 and 7. $E(\alpha)$ was calculated numerically for 500 values for α in the interval from 0° to 360°.

The number of cells N determines the radius R trough Eq. 4, permitting the calculation of the N vectors $\mathbf{r}_i$. With the coordinates x, y, z the vectors $\mathbf{t}_i$ and $\mathbf{t}_{Pi}$ are calculated for each $\mathbf{r}_i$. Then for each value of α, N values of $\mathbf{m}_{ui}(\alpha)$ are generated. For different pairs of positions $\mathbf{r}_i$ and $\mathbf{r}_j$ ($i \neq j$ and $i > j$) the energy u_{ij} is calculated assuming a value for m_0. The energy $E(\alpha)$ is calculated with all the possible values for u_{ij} and assuming an external magnetic field B_{EXT}. The entire process is repeated for the 500 values of α.

For each α the X, Y, Z components of the total magnetic moment vector $\mathbf{M}_T = \Sigma\mathbf{m}_i$ were also calculated. The process to calculate the energy depends only on three variables: the number of cells (N), the number of loops in the spherical helix (L) and the external magnetic field (B_{EXT}). The numerical results were analyzed with the Microcal Origin software. The calculations were done using values for N from 15 to 30, $L = 6$ and $B_{EXT} = 0$, 0.5 and 5,000 G.

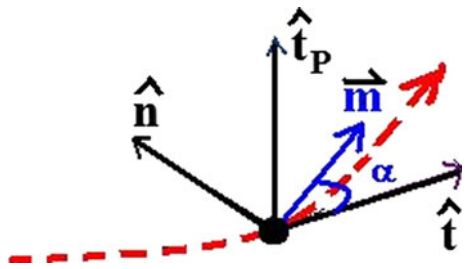

Fig. 2 Diagram of the unitary vectors used on the curve. The *dashed line* corresponds with the curve. The unitary vectors normal **n**, tangent **t** and binormal $\mathbf{t_P}$ are mutually perpendicular. The magnetic moment **m** is on the plane formed by **t** and $\mathbf{t_P}$, and makes an angle α with respect to **t**

Results

$B_{EXT} = 0$

Energy as function of α

Figure 3 shows an example of the magnetic energy as a function of the angle α. The first characteristic observed is that, independent of the N, L and R values, the energy curve presents two minima and two maxima. The minimum energy configurations have angles that differ by 180°, and also the maximum energy configurations, meaning that both configurations have their total magnetic moments aligned in the same direction but in antiparallel senses. This result is implicit in the symmetry of the dipolar energy

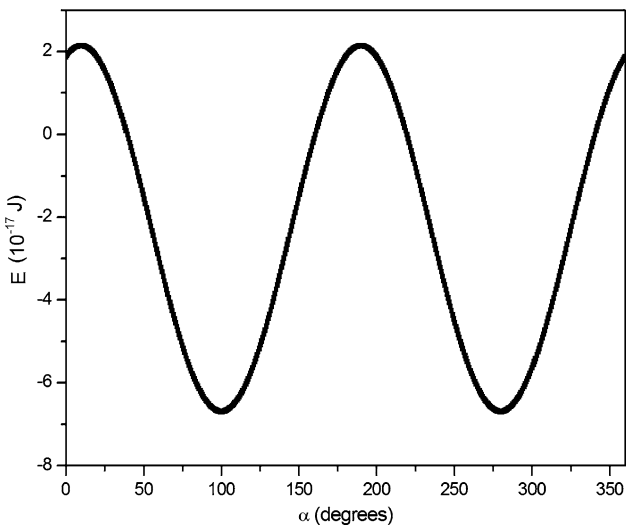

Fig. 3 Magnetic energy E for 15 magnetic moments distributed on a helix of 6 loops and $B_{EXT} = 0$, in function of the angle α as defined at Fig. 2. The radius of the CMm organism in this conditions is 1.07 μm (Eq. 4)

(Eq. 7): if $\mathbf{m}_i$ is changed to $-\mathbf{m}_i$ the magnetic energy does not change. Among adjacent minimum and maximum configurations the angles differ by 90°. In all the observed curves the minimum energy configuration is obtained for angles $\alpha \neq 0°$. In Fig. 3 the first maximum is attained at about 10° and the first minimum at about 100°. For different values of N these angles change, the maximum energy angles ranging from −30° to 30° and the minimum energy angles from 50° to 120°. In the set of minimum energies the minimum values are attained at angles at about 100°, corresponding with N values of 15, 20 and 25. After $N = 25$ the next minimum is at $N = 29$, which corresponds with an angle of about 80°. This means that the configuration that produces the minimum magnetic energy corresponds with strips of magnetic dipoles, oriented almost perpendicular to the helix turns and following approximately meridian lines (Fig. 4). This can be understood because in this discrete magnetic dipole distribution the distance among adjacent dipoles on the curve is greater than the distance between adjacent dipoles in adjacent turns. The influence of the neighbor magnetic dipole in the next turn is stronger than other neighbor dipoles. A structure like this has been proposed in magnetic self-assembly of three-dimensional surfaces from planar sheets (Boncheva et al. 2005).

The values for minimum and maximum energies were observed to be higher than the ambient thermal energy k_BT, which has a value of about 4×10^{-21} J at 300 K. To calculate the energy, a value for the magnetic moment of each cell of 1.8×10^{-15} Am^2 was assumed, as reported by Wajnberg et al. (1986).

M_{ZT} versus E

For each magnetic moment distribution, determined by the angle α, the components of the total magnetic moment vector were calculated. The most important of them is the

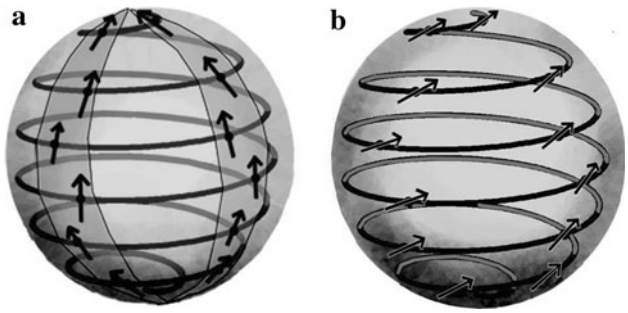

Fig. 4 CMm magnetic configurations for minimum and maximum energy. **a** Magnetic dipole chains in spherical meridians produce the minimum energy configuration (attractive). **b** Magnetic dipole rings produce the maximum energy configuration (repulsive). In both figures, *each arrow* represents the cellular magnetic dipole. The observed structure is the front one

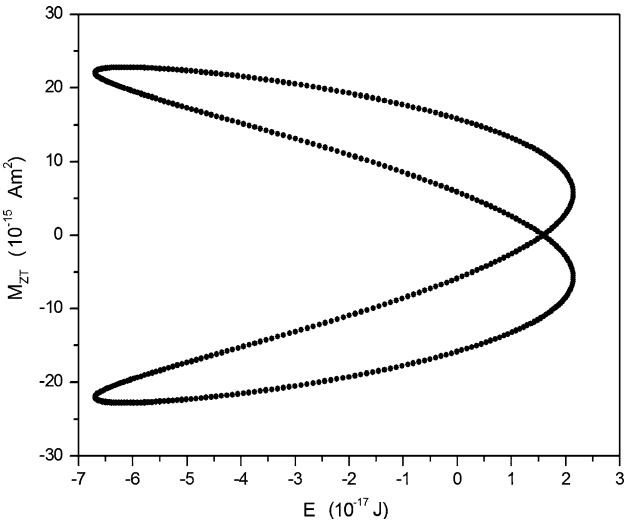

Fig. 5 Component z of the total magnetic moment (M_{ZT}) in the function of the energy E of the configuration of 15 magnetic moments distributed on a helix of 6 loops and $B_{EXT} = 0$. Observe that for each value of E there are four different values of M_{ZT} corresponding with the four different configurations with the same energy value, as is observed in Fig. 3, but for the extreme E values (minimum or maximum) there are only two different values of M_{ZT} associated to each one

z component M_{ZT}, because it is on the symmetry axis. Figure 5 shows the M_{ZT} values as a function of the energy E for $L = 6$ and $N = 15$. Similar graphs are obtained for other values of N. It is observed in Fig. 3 that four values of α produce the same value of E, but each value of α represents different distributions, producing different magnetic moment vectors, as can be observed in Fig. 5. An interesting feature is that both configurations with minimum energy have higher M_{ZT} values than those for maximum energy configurations, and M_{ZT} values for the minimum energy configurations have different polarities. As both configurations have the same minimum energy value, both polarities are possible in the same proportion for $B_{EXT} = 0$. A detailed analysis of M_{ZT} versus E curves shows that the minimum energy configurations do not have a higher value for M_{ZT} than is attained in other configurations. For example, in Fig. 5 the minimum energy is -6.692×10^{-17} J, and its corresponding M_{ZT} is $\pm 22.06 \times 10^{-15}$ Am^2, but the maximum value for M_{ZT} is 22.79×10^{-15} Am^2. The interesting feature is that the analyzed distribution does not present its maximum value for M_{ZT} at the minimum energy configuration.

Maximum and minimum energies as a function of N

As mentioned above, the magnetic configurations were analyzed with N from 15 to 30. Figure 6 shows the variation of the maximum and minimum energies as the function of N. As N grows the energy values oscillate with a

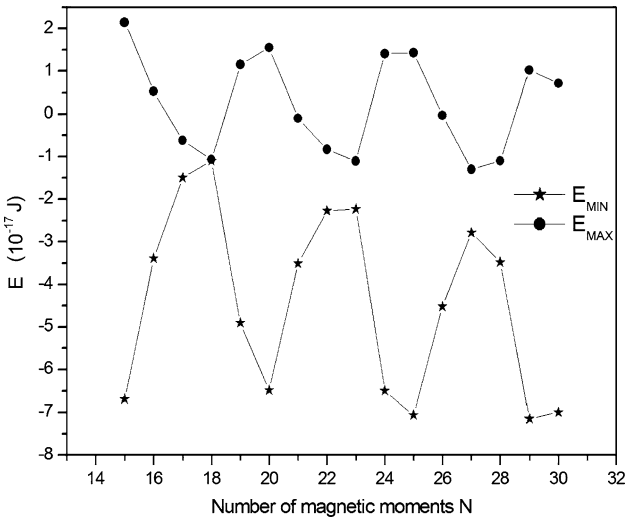

Fig. 6 Minimum and maximum values of the magnetic energy E (E_{MIN} and E_{MAX}, respectively) as a function of the number of magnetic moments N distributed on a helix of 6 loops and $B_{EXT} = 0$

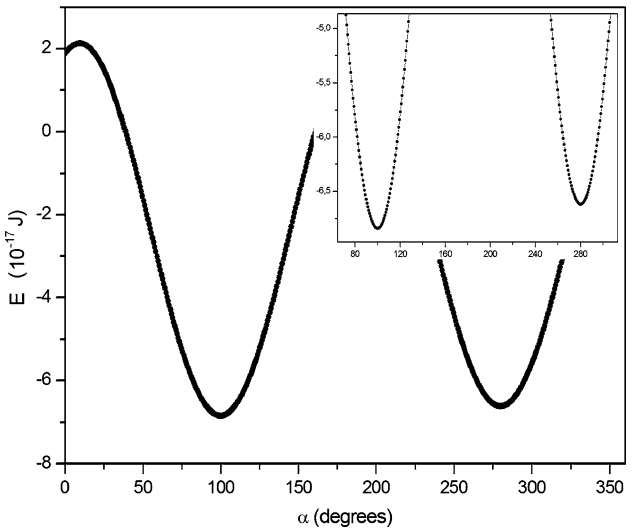

Fig. 7 Magnetic energy E for 15 magnetic moments distributed on a helix of 6 loops and $B_{EXT} = 0.5$ G, in the function of the angle α as defined in Fig. 2. The *insert* shows the difference among the minimum values of E

period of about 5. It is also observed that the configurations have two energy limits: a higher one of about 2×10^{-7} J and a lower one of about -7×10^{-7} J. For some values of N the corresponding maximum and minimum energies are very close, but never equal (in Fig. 6 for $N = 18$: $E_{MIN} = -1.09 \times 10^{-17}$ and $E_{MAX} = -1.06 \times 10^{-17}$ J). The origin of these oscillations must be the change in the relative position of the dipoles from one turn to the next as the number of cells N changes. As mentioned above, the minimum values in the oscillation for the set of minimum magnetic energies corresponds with angles of about 100° or 80°, creating a distribution of magnetic dipole chains following approximately spherical meridians. All the energy values are higher than the ambient thermal energy $k_B T$.

$B_{EXT} = 0.5$ and $B_{EXT} = 5{,}000$ G

It was observed that at $B_{EXT} = 0$ the two minimum energy configurations are degenerate in the absence of an external magnetic field. Now, the configuration energy was calculated considering $B_{EXT} \neq 0$. Figure 7 shows $E(\alpha)$ for $N = 15$, $L = 6$ and $B_{EXT} = 0.5$ G, which is about the same order of magnitude as the geomagnetic field. It was assumed that B_{EXT} is a vector directed along the z axis. As observed in Fig. 7, there are two minimum energy configurations, but with different energy values (-6.84×10^{-17} and -6.62×10^{-17} J). The magnetic field B_{EXT} removes the degeneracy and favors the configuration with a field-parallel net magnetic dipole moment (in Fig. 7, $E = -6.84 \times 10^{-17}$ J corresponds to $M_{ZT} = +22.06 \times 10^{-15}$ Am^2).

A very strong magnetic field can change this energy view. $B_{EXT} = 5{,}000$ G $= 0.5$ T is a relatively strong magnetic field, and its effect on the energy configuration is observed in Fig. 8. Now, both minimum energy configurations degenerate to only one configuration and similar to the maximum energy configurations. Figure 8 shows the result for $N = 15$ and $L = 6$, and can be compared with Figs. 3 and 7. For this strong field $E_{MIN} = -1{,}146 \times 10^{-17}$ J corresponds to $M_{ZT} = +22.79 \times 10^{-15}$ Am^2, and $E_{MAX} = 1{,}133 \times 10^{-17}$ J corresponds to $M_{ZT} = -22.79 \times 10^{-15}$ Am^2. This value of M_{ZT} for the minimum energy configuration corresponds to the greater value for M_{ZT}

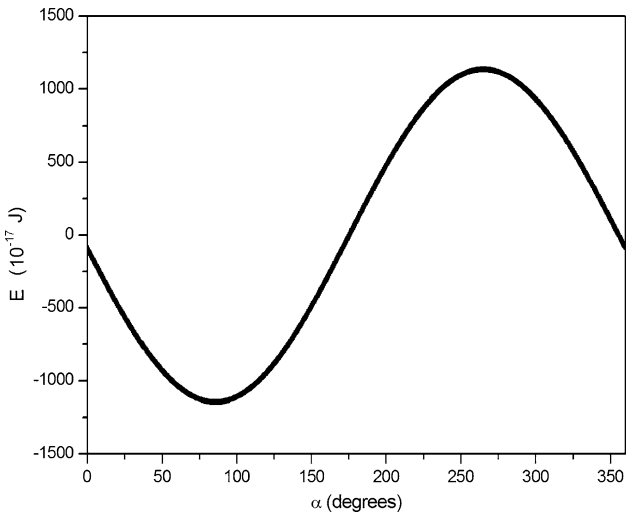

Fig. 8 Magnetic energy E for 15 magnetic moments distributed on a helix of 6 loops and $B_{EXT} = 5{,}000$ G, in the function of the angle α as defined in Fig. 2. Observe that for higher values of B_{EXT}, there are only one minimum and one maximum value for E

in the analyzed distribution with $N = 15$, $L = 6$ and $B_{EXT} = 0$.

Degree of magnetic optimization (DMO)

The values for the total magnetic moment M_T were also calculated for all the configurations. As a rule, the value of M_{ZT} is similar to the magnitude of M_T. For example, for $N = 15$ and $L = 6$ the values are $M_{ZT} = 22.79 \times 10^{-15}$ and $M_T = 22.87 \times 10^{-15}$ Am^2. Also it was observed that in the presence of a weak B_{EXT} (e.g., the geomagnetic field) the minimum energy configuration does not have the greater M_{ZT} value, but with high B_{EXT} the M_{ZT} attains its higher value. Interestingly, the greater M_T value does not correspond with the direct sum of the individual magnetic moments, which never become parallel (in the example above, the direct sum of the 15 individual magnetic moments is 27×10^{-15} Am^2). This is a consequence of the attachment to the cell structure of each individual magnetic moment, restricted to the tangent plane to the spherical body. This feature was analyzed experimentally by Winklhofer et al. (2007), where magnetic moment measurements were done with CMm using the rotating magnetic field technique, based on the swimming behavior of magnetotactic organisms in a magnetic field that rotates in the optical plane of the microscope (Hanzlik et al. 2002). In those measurements the CMm behavior was observed for two different conditions: under the natural state and after strong magnetic pulses (duration of about 2 ms and pulses with a maximum intensity of 1,000 Oe). With both measurements it is possible determine the degree of magnetic optimization (DMO), defined by Winklhofer et al. (2007) as the magnitude of the natural remanent magnetic moment in relation to the maximum remanent magnetic moment of the organism under the given boundary conditions. They determined DMO values of about 0.9 for individual organism measurements and 0.85 for measurements in groups of organisms. Our model for the magnetic structure of CMm allows the calculation of the DMO through the calculation of the magnetic energy (Eq. 5) with two different values for B_{EXT}. The natural remanent magnetic moment is obtained in the minimum energy configuration with low B_{EXT} similar to the geomagnetic field, and the maximum remanent magnetic moment is obtained with higher values of B_{EXT}. It is considered that the maximum remanent magnetic moment must be the minimum energy configuration that results from the application and removal of a high B_{EXT}. The magnetic dipole configuration remaining after the field removal must the same as that with the presence of B_{EXT}, but with a relaxation decay time to a magnetic configuration associated to weak B_{EXT}. So, for each value of N the theoretical DMO can be calculated with the quotient $M_{ZMIN}/M_{ZHIGHER}$, where M_{ZMIN} is the M_Z value at the minimum energy configuration at low magnetic fields and $M_{ZHIGHER}$ is the M_Z value for the minimum energy configuration at higher magnetic fields. Figure 9 shows the DMO value as a function of N. It is observed that the DMO value oscillates when N increases. The average DMO value for N between 15 and 30 is 0.90 ± 0.07. This average value is similar to the experimental one measured by Winklhofer et al. (2007).

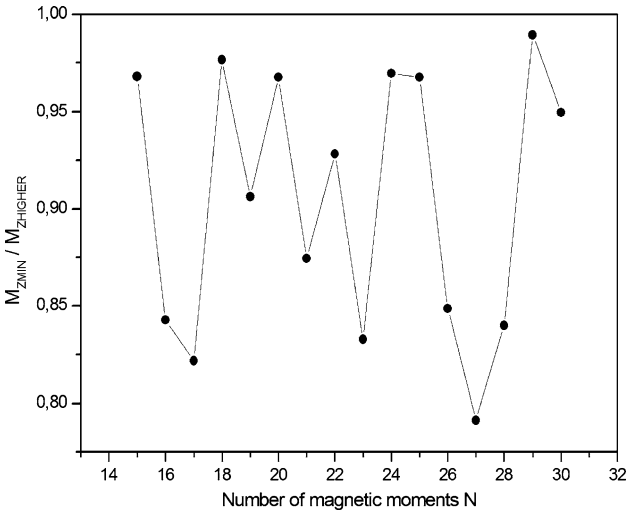

Fig. 9 Degree of magnetic optimization (DMO) as a function of the number of magnetic moments N distributed on a helix of 6 loops. The DMO was calculated through the quotient $M_{ZMIN}/M_{ZHIGHER}$, as mentioned in the paper

Discussion

The proposed model supposes that CMm has a symmetry axis with a preferred direction, corresponding to that of the resultant magnetic moment. This symmetry axis also determines the direction of movement of the organisms because of the way the flagella are distributed around the helical curve. This assumption is contrary to the soap bubble model, where a certain number of bubbles produce a spherical structure with one bubble in the center (Silva et al. 2003).

Our model is based on mathematical simplifications based on experimental observations of the CMm morphology and magnetic behavior. Several scanning electron microscopy micrographs show that CMm cells are arranged not as soap bubbles linked to form a sphere, but following a kind of spiral. Sometimes CMm seems to be formed by two spirals indicating that the cell organization is more complex or changes during the life cycle in order to maintain the cell distribution, the axis of movement and the magnetic polarity over several generations (Keim et al. 2006; Perantoni et al. 2009). So, our model starts by assuming

that CMm cells are not randomly grouped, but organized in a curve that we suppose to be a spherical helix.

In the absence of an external magnetic field ($B_{EXT} = 0$) both directions on the symmetry axis have equal probabilities to appear, but when $B_{EXT} \neq 0$ the direction parallel to the external field has higher probability. For CMm the direction parallel (antiparallel) to the geomagnetic field can be identified as the south- (north-) seeking polarity of magnetotatic organisms from the Southern hemisphere (Bazylinski and Frankel 2004). As can be observed in Fig. 7, the parallel configuration is preferred to the antiparallel one, but the energy levels are so close that it is possible that organisms with both polarities coexist in the same population. The presence of CMms with both polarities in the same population has been observed in samples collected at Araruama Lagoon in Rio de Janeiro, Brazil (Keim et al. 2006). The polarity change has also been observed in remagnetization experiments, exposing the organisms to a 60-Hz AC magnetic field (Rodgers et al. 1990; Keim et al. 2006).

The model also proposes a magnetic organization not seen in any other living organism. The CMm magnetic organization was proposed by others (Abreu et al. 2007; Rodgers et al. 1990; Keim et al. 2006; Winklhofer et al. 2007; Perantoni et al. 2009), but for the first time the idea was used here in a consistent model to calculate the optimal distribution of magnetic moments and the magnetic energy configurations. One can speculate whether the helical distribution can be the ultimate result of the magnetic interaction between the CMm cells. It is difficult to demonstrate that N magnetic moments, free to interact between them, have an equilibrium distribution in a spherical helix. Theoretical studies of the dynamics of fragmentation of magnetic structures show that rings of magnetic nanoparticles, in the presence of magnetic fields perpendicular to the ring plane, disrupt into helical chains when the intensity of the magnetic field increases (Jund et al. 1995). Experiments on the three-dimensional self-assembly of metallic rods with submicron diameters, using magnetic interactions, showed that they form "bundles" of rods, each rod oriented side-by-side with their long axes parallel to one another and their ferromagnetic sections aligned. The metallic rods were designed to contain two ferromagnetic sections separated by diamagnetic sections. The ferromagnetic sections were constructed in such a way that the easy axis of magnetization is perpendicular to the long axis of the rod. This restriction permits the formation of stable "bundles". They observed that the magnetic dipoles in a bundle are ordered such that the bundle has little or no net magnetic dipole (Love et al. 2003). This experiment shows that the natural 3D assembly of magnetic objects produces structures with no net magnetic dipole. The high DMO observed in CMm organisms is contrary to that result. The 3D geometrical organization through the spherical helix favors a magnetic structure with minimum magnetic energy and with a high resultant magnetic moment. That must be of biological relevance for an agglomerate of magnetotactic bacteria: the spherical helix permits that the resultant organism maintains the magnetic behavior.

The present model showed minimum energy configurations of magnetic moments in spherical meridian chains, perpendicular to the helix turns. These configurations are compatible with the observed highly ordered arrangement of the magnetosome chains across entire MMP organisms from North Sea sediments (Wenter et al. 2009). Figure 2b and c from Wenter et al. (2009) shows the chains of magnetosomes following meridians and almost perpendicular to the helix observed at Fig. 2a of the same reference.

In the model we assumed that all the magnetic moments have the same inclination with respect to the curve. For the CMm organism that supposition is supported by the fact that there is a relation among the position of the magnetosome chain and the flagella. If all the bacteria composing the CMm body are similar, having their flagella following the spiral, then all the magnetic moments associated with each bacterium must have the same inclination with respect to the spiral curve.

The organism *Candidatus* Magnetoglobus multicellularis shows a high degree of magnetic and biological organization (Abreu et al. 2007; Wagensberg et al. 2010). It is composed by several bacteria, but behaves as a single organism. It does not show a unicellular division process but a coordinate binary division of the whole organism. A parameter to characterize the optimization of this magnetic organization is the degree of magnetic optimization (DMO). Through the distribution of magnetic moments on a spherical helix, inclined with respect to the curve line, it was possible to obtain DMO values similar to the experimental ones (Winklhofer et al. 2007). The high DMO shows that its geometrical structure is important to maintain the magnetotactic behavior. Magnetic forces do not have to be responsible for this structure, but our model indicates that the helical structure must have magnetic significance.

Our model also shows that the magnetic energy associated with the minimum energy configuration is higher than the thermal energy, not suffering from instabilities of the local temperature, adapting easily to different weather all over the world.

This model should be applied to analyze the division process proposed for this organism by Keim et al. (2004b), where it divides in a binary fashion, following a set of geometrical surfaces similar to that obtained through rotation of Cassini curves.

Acknowledgments We thank to Dr. Donald E. Ellis for comments on and corrections of the manuscript. We acknowledge financial support from the Brazilian agency CNPq.

References

Abreu F, Martins JL, Silveira TS, Keim CN, Lins de Barros HGP, Gueiros Filho FJ, Lins U (2007) "*Candidatus* Magnetoglobus multicellularis", a multicellular, magnetotactic prokaryote from a hypersaline environment. Int J Syst Evol Microbiol 57:1318–1322

Bazylinski DA, Frankel RB (2004) Magnetosomes formation in prokaryotes. Nat Rev Microbiol 2:217–229

Boncheva M, Andreev SA, Mahadevan L, Winkleman A, Reichman DR, Prentiss MG, Whitesides S, Whitesides GM (2005) Magnetic self-assembly of three-dimensional surfaces from planar sheets. Proc Natl Acad Sci USA 102:3924–3929

Farina M, Lins de Barros H, Esquivel DMS, Danon J (1983) Ultrastructure of a magnetotactic microorganism. Biol Cell 48:85–88

Farina M, Esquivel DMS, Lins de Barros HGP (1990) Magnetic iron-sulphur crystals from a magnetotactic microorganism. Nature 343:256–258

Fleming A, James R (2011) School of Physics. The University of Western Australia. Web. 11 August 2011. http://www.biophysics.uwa.edu.au/STAWA/

Frankel RB (2003) Biological permanent magnets. Hyperfine Interact 151(152):145–153

Hanzlik M, Winklhofer M, Petersen N (2002) Pulsed-field-remanence measurements on individual magnetotactic bacteria. J Magn Magn Mat 248:258–267

Jund P, Kim SG, Tomanek D, Hetherington J (1995) Stability and fragmentation of complex structures in ferrofluids. Phys Rev Lett 74:3049–3052

Keim CN, Abreu F, Lins U, Lins de Barros H, Farina M (2004a) Cell organization and ultrastructure of a magnetotactic multicellular organism. J Struct Biol 145:245–262

Keim CN, Martins JL, Abreu F, Rosado AS, Lins de Barros HGP, Borojevic R, Lins U, Farina M (2004b) Multicellular life cycle of magnetotactic prokaryotes. FEMS Microbiol Lett 240:203–208

Keim CN, Martins JL, Lins de Barros H, Lins U, Farina M (2006) Structure, behavior, ecology and diversity of multicellular magnetotactic prokaryotes. In: Schuler D (ed) Magnetoreception and magnetosomes in Bacteria. Springer, Berlin, Heidelberg, pp 103–132

Lins de Barros HGP, Esquivel DMS (1987) An upper size limit to magnetotactic microorganism. Studia Biophysica 121:55–64

Lins U, Farina M (1999) Organization of cells in magnetotactic multicellular aggregates. Microbiol Res 154:9–13

Lins U, Kein CN, Evans FF, Farina M, Buseck PR (2007) Magnetite (Fe_3O_4) and greigite (Fe_3S_4) crystals in multicellular magnetotactic prokaryotes. Geomicrobiol J 24:43–50

Love JC, Urbach AR, Prentiss MG, Whitesides GM (2003) Three-dimensional self-assembly of metallic rods with submicron diameters using magnetic interactions. J Am Chem Soc 125:12696–12697

Mann S, Sparks NHC, Frankel RB, Bazilinski DA, Jannash HW (1990) Biomineralization of ferromagnetic greigite (Fe_3S_4) and iron pyrite (FeS_2) in a magnetotactic bacteria. Nature 343:258–261

Perantoni M, Esquivel DMS, Wajnberg E, Acosta-Avalos D, Cernicchiaro G, Lins de Barros H (2009) Magnetic properties of the microorganism Candidatus Magnetoglobus multicellularis. Naturwissenschaften 96:685–690

Rodgers FG, Blakemore RP, Blakemore NA, Frankel RB, Bazylinski DA, Maratea D, Rodgers C (1990) Intercellular structure in a many-celled magnetotactic prokaryote. Arch Microbiol 154:18–22

Silva KT, Keim CN, Abreu F, Martins JL, Rosado AS, Farina M, Lins U (2003) Spatial relationships of cells within magnetotactic multicellular aggregates. Acta Microscopica 12 (Suppl B):367–368

Wagensberg J, Garcia Leal A, Lins de Barros HGP (2010) Individuals versus individualities: a Darwinian approach. Biol Theory 5(1):87–95

Wajnberg E, Salvo de Souza LH, Lins de Barros HGP, Esquivel DMS (1986) A study of magnetic properties of magnetotactic bacteria. Biophys J 50:451–455

Weisstein EW (2011a) Spherical helix. In: Mathworld—A Wolfram web resource. Web. 03 February 2011. http://mathworld.wolfram.com/SphericalHelix.html

Weisstein EW (2011b) Spherical spiral. In: Mathworld—"A Wolfram web resource. Web. 03 February 2011. http://mathworld.wolfram.com/SphericalSpiral.html

Wenter R, Wanner G, Schuler D, Overmann J (2009) Ultrastructure, tactic behaviour and potential for sulfate reduction of a novel multicellular magnetotactic prokaryote from North Sea sediments. Environ Microbiol 11:1493–1505

Winklhofer M, Abraçado LG, Davila AF, Keim CN, Lins de Barros HGP (2007) Magnetic optimization in a multicellular magnetotactic organism. Biophys J 92:661–670

Zhou K, Pan H, Zhang S, Yue H, Xiao T, Wu L (2011) Occurrence and microscopic analyses of multicellular magnetotactic prokaryotes from coastal sediments in the Yellow sea. Chin J Oceanol Limnol 29:246–251